 doi:10.20944/preprints201701.0062.v1

Article

An Adaptive Self-powered Piezoelectric Energy Harvesting Circuit and Its Application on Bridge Condition Monitoring

Teng Li [1,*], Yunxin Zhang [2] and Xinlai Geng [1]

[1] Beijing Jiaotong University, Beijing 100044, China
[2] China Power Purui Electric Power Engineering Co. Ltd, Beijing, China
* Correspondence: liteng@bjtu.edu.cn; Tel.: +86-10-51685212

Abstract: The abundant mechanical vibration energy in bridge road environment can be converted into electric energy by using the piezoelectric energy harvest technology, which could be an efficient way to provide energy required by the wireless sensor network in the bridge condition monitoring system. An autonomous energy harvesting system has been designed based on cantilever beams for sensing and acquiring the bridge vibration energy. After the analysis of the dynamic properties of the piezoelectric cantilever beam in the energy conversion, three kinds of interface circuits were compared through simulation and experimental results. It was shown that the VD interface circuit has less power loss. Furthermore, the proposed closed loop control method based on the VD circuit was simple, adaptive, and self-powered, which is suitable for the road energy harvesting application. Finally, the energy harvesting system based on VD circuit was realized with harvested power of around 0.8mW.

Keywords: piezoelectric cantilever energy harvester 1; autonomous 2; adaptive 3; self-powered 4; voltage doubler interface circuit 5; closed loop control 6; feed-forward 7; multi-shot technology 8

1. Introduction

The vibration energy is huge in the environment and human body itself. Researchers in the MIT Media lab have investigated power-harvesting from running shoes [1, 2] as a method of generating power for wearable electronics. A piezoelectric bender placed in the sole, which flexes during the human gait; a piezoelectric unimorph attached to a curved steel plate, which flexes under the pressure of a heel strike. The piezoelectric sole and heel generators produce around 2 and 8 mW, respectively.

Besides human body vibration energy, piezoelectric transducer can also be used for acquiring environmental energy, which can be supplied to wireless health monitoring sensors installed in different constructions. For example, Roundy and Wright developed a piezoelectric energy harvesting system for providing power needed by wireless sensors[3] . Experimental results showed that the energy of 375μW produced by the piezoelectric element met the power supply requirement of the wireless sensor. Studies about the low-power wireless sensor module applied in the structural health monitoring have been performed [4, 5]; experimental results showed that when the wireless sensor in sleep mode, the power consumption of μW-level can be achieved, while the power consumption in the work mode for the sensor reached mW-level [5]. Compared to the building vibration energy mainly from the human activities, vibration energy comes from the automobiles are much larger. Research showed that the vibration in the highway of Tokyo can generate the electricity of 4GW,

 doi:10.20944/preprints201701.0062.v1

satisfying the requirements of 3.4 million residence. The Innowattech company in Israel buried piezoelectric energy harvesting transducers under the asphalt road of 6cm, and the interval distance of transducers were 30cm. Experimental results showed that, when a truck with the weight of 12 tons passed through the road with transducers buried at both sides for 10 meters, electricity of 1 kilowatt-hour would be generated[6]. Besides harvesting the energy, these transducers with the name of 'Weighing In Motion' can also be used to measure the traffic flow, car speed and car load[7].In the technology using piezoelectric energy for powering wireless sensor, A bridge wireless monitoring technique presented based on traffic vibration energy harvesting, which was tested on a 1 km long New Carquinez bridge in California and showed an average power of 0.5-0.75μW for the power usage of wireless sensing[8]. Researchers from UK reported the vibration energy harvesting device combined both direct resonance and parametric resonance in order to improve harvesting efficiency adapting to real-world ambient vibration[9]. The designed electromagnetic harvester was tested in situ on the bridge, and it was capable of recovering in excess of 1 mW average raw AC power from the traffic-induced vibrations in the lateral bracing structures underneath the bridge deck.

There are mainly three possible methods of piezoelectric, electromagnetic, and electrostatic, to convert ambient vibration/motion energy into electrical energy [10].To maximize the harvested vibration energy, methods based different effects such as piezoelectric and electromagnetic have been combined[11].One main advantage of piezoelectric energy harvesting methods is the ability to produce significant output voltages in the 10 to 100 V range, which is useful in minimizing the effects of voltage drops required for typical rectification. Whereas electromagnetic methods were typically confined to the mV range[10]. Also, unlike the electrostatic method, piezoelectric energy harvesting can operate without an external power source for transduction[10].

For the piezoelectric energy harvesting in the low frequency range below hundred Hertz, at present, most of piezoelectric transducers were made of PZT-5H piezoelectric ceramics for its high effective electro-mechanical coupling coefficient and strain constants compared to other PZT materials[12]. Different structures were used in different applications to maximize the harvesting efficiency including structures of ceramic plates, ceramic cantilever beams, piezoelectric drums, piezoelectric cymbals and multilayer ceramics. The piezoelectric unimorph and bimorph plates have a wide range of resonant frequency usually from 5Hz to 100Hz, and they were commonly used in the vibration energy harvesting structure of the cantilever beam. To increase the generated power, a plurality of elements can be connected electrically in parallel to increase the output current of the transducer, and piezoelectric stack is such kind of structure[10] . It is suitable for harvesting low frequency unidirectional vibration, and is easy to be installed. However, energy can only be generated if the force is applied longitudinally, so the structure would not be very good to be used in applications where bending is used as a stress inducer. Also, the volume of piezoelectric stack is usually large[10] . Cymbal type piezoelectric plate can withstand a relatively large stress, producing greater strain, and resulting in a higher output charge level; it also has an adjustable resonant frequency. However, the structure is relatively complex. In summary, a single piezoelectric power generation unit generally outputs a voltage with amplitudes of 5 to 20 volts, and the current at the same time reaches to milliampere level. Thus the output power up to tens of milliwatts meets the requirement of a wireless network sensor or any other low energy-consuming electronic product with the similar energy demand. In this paper, a piezoelectric cantilever beam has been applied to harvest vibration energy.

The output voltage of the piezoelectric element is alternating, instantaneous and random, its amplitude and frequency are related to many factors such as the vibration excitation level and frequency, the size and shape of the piezoelectric element. For example, effects of mass, mass moment inertia, and mass center offset of a proof mass on the electrical power harvesting

 doi:10.20944/preprints201701.0062.v1

are significant[13]. However, this paper mainly focused on the circuit design of the energy harvesting system other than the piezoelectric element itself.

The electrical signal converted by piezoelectric element is an AC signal. In order to provide continuous and stable power supply to wireless sensors or electronic devices, an interface circuit between the piezoelectric element and the voltage regulating circuit was usually need to convert the AC to DC voltage. The interface circuit is directly related with the energy harvesting efficiency. In addition, energy storage units are required[13]. The maximum output power on the load should also be the criteria for the interface circuit design.

In 2002, Ottman et al. proposed the standard interface circuit in the energy harvesting system [14]. The interface circuit consisted of a full-bridge rectifier circuit and a filter capacitor, relationship between the interface output voltage, the open-circuit voltage of the piezoelectric element, and the load has been derived. The maximum energy has been obtained through matching the load. Guyomar et al. [15] proposed a parallel Synchronized Switch Harvesting on Inductor (p-SSHI) interface circuit [16]. Based on the standard interface circuit, a synchronous switching inductor was connected in parallel with the piezoelectric element. When the output voltage of the piezoelectric element reached the maximum value, the switch was closed, and the output power of the piezoelectric plate could be increased by controlling the synchronous switch inductor. When the inversion coefficient of the inductor was between 0.5 and 0.8, the maximum output power could reach the value of more than 4 times of the standard circuit [16]. Taylor et al. [15] proposed a series-connected Synchronized Switch Harvesting on Inductor (s-SSHI) technique[17] that connected the synchronous switching inductor with a piezoelectric element in series. The output power of s-SSHI was similar with the p-SSHI interface circuit, but the optimal resistance was about one fourth of the p-SSHI interface. Lefeuvre et al proposed a Synchronous Electric Charge extraction (SECE)circuit; theoretically, the output power of the interface circuit is not related with the output resistance, and the output power of SECE was 4 times of the maximum output power of the standard interface circuit[18]; Ottman and Lesieutre et al. studied the buck DC-DC converter energy harvesting circuit, experiments showed that with the variation of the magnitude of the exciting force, the efficiency of the step-down voltage converter changed in the range of 0-70%. When the output voltage of the piezoelectric element was 48V, the efficiency of the circuit was 3.25 times than that of the standard circuit; when the open circuit voltage of the piezoelectric element was 50V, the conversion efficiency of the step-down DC-DC circuit reached the maximum value of 70%. Lallart et al. proposed a Double Synchronized Switch Harvesting (DSSH) circuit. Based on the circuit of SSHI, a boost-buck converter was added in the circuit to make the output power irrelevant to subsequent load. The output power of the DSSH was 5 times more than the maximum output power of the standard circuit[19]. However, there was the need of using a DSP control system, and the power consumption for the DSP control hasn't been taken into account. So there was a gap away from the realization of circuit self-sufficiency. Chen experimentally compared above circuits, and designed a self-powered SSDI (synchronized switching damping on an inductor) circuit [20]. Based on DSSH circuit, an Enhanced Synchronized Switch Harvesting (ESSH) circuit has been proposed. The circuit topology was the same as that of the DSSH circuit, but the switch control was different. The switch in DSSH circuit was off at the end of the voltage transfer, and the switch in ESSH circuit was off when the capacitor voltage reached to a certain value. ESSH circuit greatly optimized the performance the interface circuit, improved the efficiency of the battery charge. Voltage doubler (VD) interface is a simple circuit compared to other interface circuits, and it has lower power dissipation compared to the standard circuit. Not only it has only two diodes for the voltage rectification, thus less voltage drops; but also it doubles the output voltage to the twice of the input voltage, thus the load current will be smaller and cause less power consumption. Energy harvesting circuit based on voltage doubler (VD) interface circuit had also a relatively high efficiency of around 60%[21, 22]. However, the open loop control of the VD circuit was a

Preprints (www.preprints.org) | NOT PEER-REVIEWED | Posted: 12 January 2017 doi:10.20944/preprints201701.0062.v1

pseudo-adaptive control since the reference voltage had to be adjusted manually and continuously to adapt the variation of the input voltage; Furthermore, it is not suitable to the application with the energy storage component since the output voltage of the DC-DC circuit was not regulated.

Five commonly used interface circuits, standard, p-SSHI, s-SSHI, SECE, and VD interface circuits will be compared theoretically at the beginning of this paper. Three of them, the standard, p-SSHI and VD circuits have been realized to verify the theoretic comparison conclusion. Then a new closed loop control circuit based on VD interface has been proposed for adaptively obtaining the vibration energy and providing for the power supply for the varying load. The whole circuit is also a self-powered stand-alone system.

2. Materials and Methods

2.1. Design of the cantilever beam

The natural frequency of the piezoelectric cantilever used for the bridge road energy harvesting should be close to the resonant frequency of the bridge road. Vibration amplitude and frequency not only relate with the material structure of the road, but also with the traffic load and speed; so the vibration amplitude and frequency for road energy harvesting is in a wide range. It has been shown that the resonant frequency of urban roads with asphalt pavement was about 20Hz[23, 24]. For the bridge condition monitoring, the main resonant frequencies of the bridge deck were identified in the range from 0-50Hz by installing energy harvester on the girders and the pipe fixed on the girders under a bridge in France, where the power spectral densities have the peak values at the frequencies around 14.5Hz[25]. Another research showed the active frequency range for harvester installed on the lateral bracings of a bridge was 7-26Hz[9].

There were other reports of scavenging the energy from the railway using the piezoelectric devices, where installed under the rails or sleepers. Frequencies detected using piezoelectric devices had low frequencies below 30Hz[26]. We can see the traffic caused vibrations are in a wide range, depending on the piezoelectric element and bridge structures, the installation positions, and the traffic flow. In this paper, the first-order natural frequency of a designed piezoelectric cantilever beam was around 20Hz.

The sketch of the piezoelectric cantilever vibration is shown in Figure 1(a). The photo of a homemade piezoelectric cantilever is shown in Figure 1(b). The piezoelectric cantilever model was composed of a piezoelectric layer and an elastic non-piezoelectric layer with one end fixed. The sketch of the beam vibration is shown in Figure 1(a). The lengths of substrate and piezoelectric material were made almost the same to increase the output power[27]. PZT-5H piezoelectric material and the substrate copper material were connected through the conductive adhesive bonding. The material parameters are shown in Table 1 and Table 2. The length, width and thickness of the base beam are respectively 60mm, 30mm and 0.3mm.

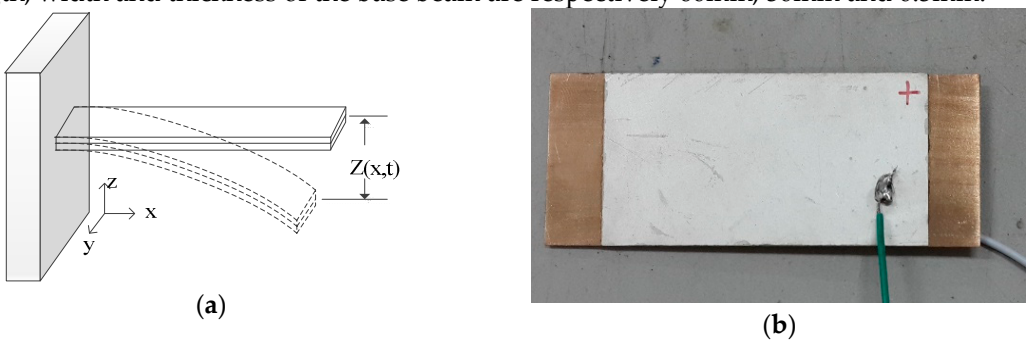

(**a**) (**b**)

Figure 1. (**a**) Sketch of the piezoelectric cantilever vibration; (**b**) Actual piezoelectric cantilever.

Table 1. Copper material parameters [28]

Preprints (www.preprints.org) | NOT PEER-REVIEWED | Posted: 12 January 2017 doi:10.20944/preprints201701.0062.v1

Material	Yong's modulus	Poisson's ratio	Density
Copper	$11*10^{10}\ Pa$	0.35	$8700\ Kg/m^3$

Table 2. Piezoelectric material parameters[28]

Material	Density Kg/m^3	Flexibility constant $10^{-12}\ m^2/N$						Piezoelectric constant $10^{-12}\ C/N$			Relative dielectric constant	
		S_{11}	S_{33}	S_{44}	S_{12}	S_{13}	S_{66}	D_{31}	D_{33}	D_{15}	ε_{11}	ε_{33}
PZT5H	7500	16.5	20.7	43.5	4.78	8.45	42.6	-186	670	660	3130	3400

According to the analytic solutions of the beam motion equation, the second-order natural frequency of the beam was around 160Hz, much larger than the bridge vibration frequency. Furthermore, the beam was made with fragile material, the second order and above natural frequencies can cause severe bend, or further damage of the beam. Thus, the piezoelectric cantilever beam was designed based on the first order natural frequency.

Modal analysis of the designed three dimensional unimorph cantilever has been performed by the finite element software of COMSOL[28], its first-order natural frequency vibration mode is shown in Figure 2(a). Using solid mechanics module, the left side end of the beam was fixed, and the right side end was added with a proof mass to increase effective mass and decrease the damping with a freely move. The mass value was 13.6g. The eigen frequency analysis was done. The resonant response of the beam was also analyzed to obtain the relationship between the output voltage and the vibration frequency. In the simulation, the sinusoidal vibration excitation with displacement of 0.2mm was applied to the left end of the cantilever, and the open circuit voltages near the first order natural frequency were obtained, which is shown as a black line in Figure 3. The simulated first order natural frequency was 25.1Hz. The response of the homemade cantilever has been tested; the test photo is shown in Figure 2(b). However, the experimental result of the beam resonant response, which was plotted as a red line in Figure 3, shows that the natural frequency of the real beam was 21Hz. The deviation between theoretical and test values may be caused by following factors. First, the conductive adhesive between the piezoelectric ceramic material and the substrate copper could decrease the damping frequency. Second, there were some differences of the parameters between the actual piezoelectric ceramic material and the theoretical one.

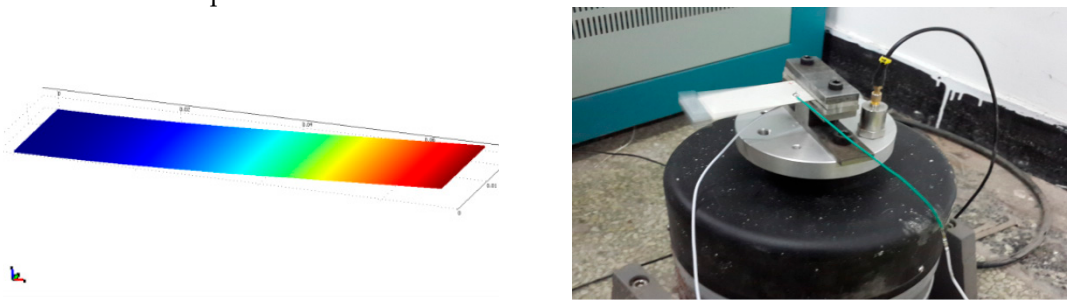

(**a**) (**b**)

Figure 2. (**a**) First-order natural frequency vibration mode of the beam simulated by COMSOL; (**b**) Experimental test of the beam.

Preprints (www.preprints.org) | NOT PEER-REVIEWED | Posted: 12 January 2017 doi:10.20944/preprints201701.0062.v1

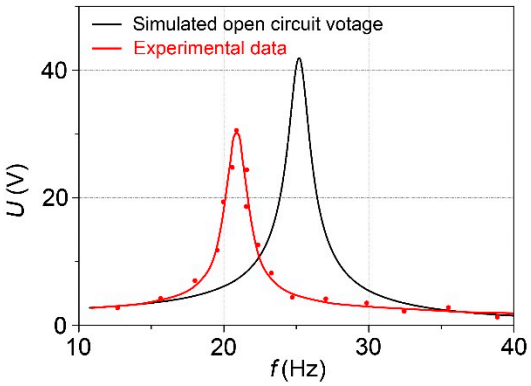

Figure 3. Simulated and experimental open-circuit voltages near the first-order natural frequency

2.2. Equivalent circuit of the cantilever harvester

A single-degree-of-freedom (SDOF) cantilever can be simplified to a mass-spring-damper system shown in Figure 4(a)[13], it describes well the behavior of the vibration-powered electrical generator. The electromechanical structure of this system is a piezoelectric beam, the top of the beam is bonded on the mass *M*, and the bottom end is bonded on the rigid base. The stiffness and the losses of the mechanical part are represented by a spring *Ks* and viscous damper *C* in this model. The rigid mass *M* undergoes both external and internal forces. The external force F results from the mechanical excitation applied on the structure. The internal force includes restoring forces due to the piezoelectric element and the spring, and a viscous force due to the damper. The mass displacement is *u*. When the energy conversion structure works in the resonant state, the energy output by the piezoelectric element can be maximized.

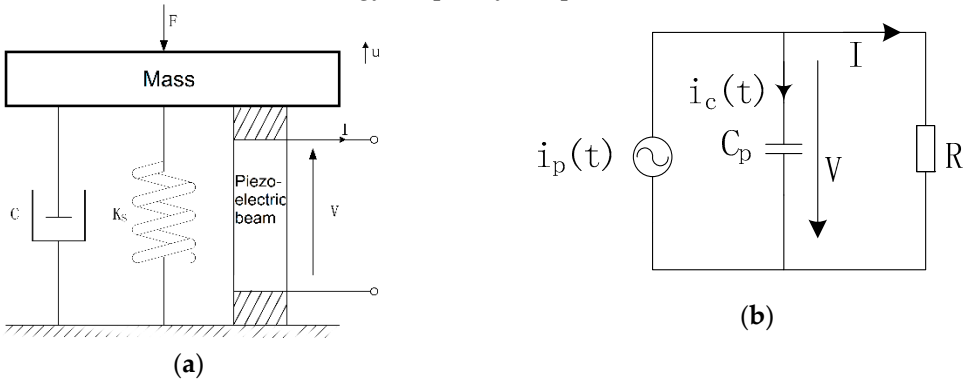

Figure 4. (**a**) SDOF model of the piezoelectric cantilever; (b) Equivalent circuit of the cantilever.

The piezoelectric beam can be equivalent to a sinusoidal current source $i_p(t)$ and a capacitor C_p shown in Figure 4(b)[10, 13]. The relationship of the current source the displacement is shown in equation (1):

$$i_p(t) = \alpha \frac{du}{dt} \quad , \tag{1}$$

Where a is the force factor, a coupling term between the force, the electrostatic energy on the piezoelectric element and the energy transferred to the electrical system[29].w is the vibration angular frequency and U_M is the maximum structural displacement.

Suppose the mechanical vibration of the piezoelectric beam is:

Preprints (www.preprints.org) | NOT PEER-REVIEWED | Posted: 12 January 2017 doi:10.20944/preprints201701.0062.v1

$$u = U_M \cos \omega t \quad , \tag{2}$$

If the beam is connected with a load, which is shown in Figure 4(b), then the current flow through the load will be:

$$I = \alpha \omega U_M \sin \omega t - C_p \frac{dV}{dt} \quad , \tag{3}$$

The first item in the equation (3) is the current source i_p(t), and the second item is the capacitor current.

When the beam is open-circuited, the current I will be zero. From equation (3), we can get the open circuit voltage:

$$V = \frac{\alpha U_M}{C_P} \cos \omega t \quad , \tag{4}$$

From equation (4), we can see that the peak value of the open circuit voltage is related to a, U_M and C_p.

2.3. Interface circuits

The output power, the maximum output power and the optimal output resistance are analyzed theoretically for the standard interface circuit, the p-SSHI interface circuit, the s-SSHI interface circuit, the SECE interface circuit and the VD interface circuit[13, 29-32]. Schematics of these five circuits are shown in the Figure 5. According to the formulas listed in Table 3, normalized output power curves regarding to the normalized load resistance of five circuits are plotted in the Figure 6(a). In the calculation, we suppose the equivalent capacitance C_p is 150nF，vibration frequency f is 20Hz, and the structural displacement amplitude U_M is 0.2mm, corresponding to the peak amplitude of the current source of 0.566mA. 'Normalized' output power means the output powers versus the load were divided by the maximum output power of the standard interface circuit. 'Normalized' load means the load resistances were divided by the optimal load of the standard interface circuit. Figure 6(b) also shows the normalized output power curves of p-SSHI (red lines) and s-SSHI (green lines) circuits when their quality factors were changed. Quality factor is related to the oscillation frequency caused by R, L and C in the circuits.

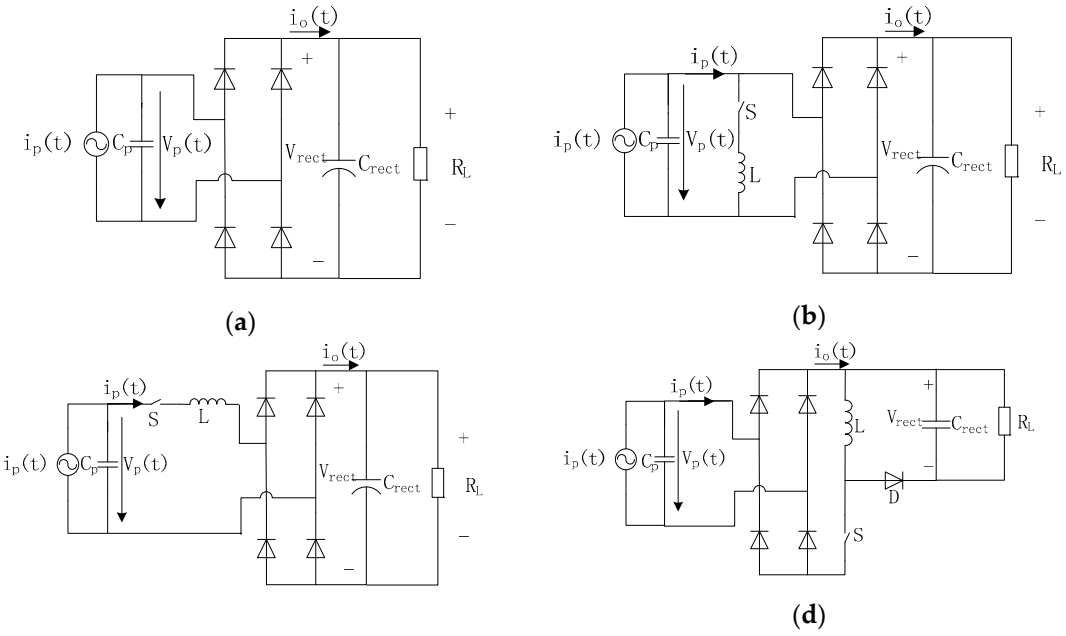

Preprints (www.preprints.org) | NOT PEER-REVIEWED | Posted: 12 January 2017 doi:10.20944/preprints201701.0062.v1

(c)

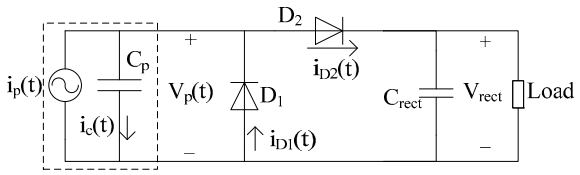

(e)

Figure 5. Energy harvesting interface circuits: (a) Standard interface circuit; (b) p-SSHI interface circuit; (c) s-SSHI interface circuit; (d) SECE interface circuit; (e) VD interface circuit [13].

Table 3. Output powers, maximum output powers and optimal loads of five interface circuits[10, 13]

Circuits	Output Power	Maximum output power	Optimal load
Standard	$\frac{R_L\alpha^2\omega^2U_M^2}{\left(R_LC_P\omega+\frac{\pi}{2}\right)^2}$	$\frac{\omega\alpha^2U_M^2}{2\pi C_P}$	$\frac{\pi}{2C_P\omega}$
p-SSHI	$\frac{4R_L\alpha^2\omega^2U_M^2}{\left(R_LC_P\omega\left(1-e^{-\frac{\pi}{2Q_i}}\right)+\pi\right)^2}$	$\frac{\omega\alpha^2U_M^2}{\pi C_P\left(1-e^{-\frac{\pi}{2Q_i}}\right)}$	$\frac{\pi}{C_P\omega\left(1-e^{-\frac{\pi}{2Q_i}}\right)}$,
s-SSHI	$\frac{4R_L\alpha^2\omega^2U_M^2\left(1+e^{-\frac{\pi}{2Q_i}}\right)^2}{\left[\pi\left(1-e^{-\frac{\pi}{2Q_i}}\right)+2\omega R_LC_P\left(1+e^{-\frac{\pi}{2Q_i}}\right)\right]^2}$	$\frac{\omega\alpha^2U_M^2\left(1+e^{-\frac{\pi}{2Q_i}}\right)}{2\pi C_P\left(1-e^{-\frac{\pi}{2Q_i}}\right)}$	$\frac{\pi\left(1-e^{-\frac{\pi}{2Q_i}}\right)}{2C_P\omega\left(1+e^{-\frac{\pi}{2Q_i}}\right)}$,
SECE	$2\frac{\omega\alpha^2U_M^2}{\pi C_P}$	----------	----------
VD	$\frac{4\alpha^2\omega^2R_LU_M^2}{(\omega R_LC_P+2\pi)^2}$	$\frac{\omega\alpha^2U_M^2}{2\pi C_p}$	$\frac{2\pi}{C_p\omega}$

As can be seen from Figure 6, the output powers of four circuits are related to the load except the SECE circuits. The maximum out power of the standard interface circuit equals to the VD interface circuit; the maximum output power of the p-SSHI circuit is slightly larger than the s-SSHI circuit; and the maximum output powers of the SSHI interface circuits are greater than the standard interface circuit. That means the synchronous switch inductance circuit can effectively increase the output power of the circuit.

The load value corresponding to the maximum output power is called the optimal load. From Figure 6(a), we can also see the optimal loads of the VD and the p-SSHI circuits are

Preprints (www.preprints.org) | NOT PEER-REVIEWED | Posted: 12 January 2017 doi:10.20944/preprints201701.0062.v1

larger than the standard circuits; the optimal load of the s-SSHI circuit is smaller than the standard circuit. There is no power change regarding to the load for the ideal SECE circuit. Figure 6 (b) shows the normalized output power curves of the p-SSHI and s-SSHI interface circuits when changing their quality factors in the range of 2 to 4. With the increase of the quality factor, the output powers of the p-SSHI and s-SSHI circuits are also increased. In addition, the optimal load of the p-SSHI circuit increases with the increase of the quality factor; and the optimal load of the s-SSHI circuit decreases with the increase of the quality factor. Wireless network sensors correspond to loads with wide range, thus p-SSHI is preferred in the condition motoring application than s-SSHI. Theoretically, the output power of SECE is not changed with the load. However, the output power of SECE indeed decreased during the high load range in experiment tests and the maximum power was hard to reach 4 times of the standard circuit[31]. In some cases, the SECE circuit may lead to harvested powers lower than the standard circuit with vibrations composed of a low-frequency mode with large amplitude, mixed with a high-frequency mode with weak amplitude[31]. Difference between theoretical and experimental power gains may be due to the piezoelectric material leakage resistance which was not considered in the model[31]. Thus, for the bridge monitoring applications, we will mainly consider three circuits of the standard, p-SSHI and VD circuits.

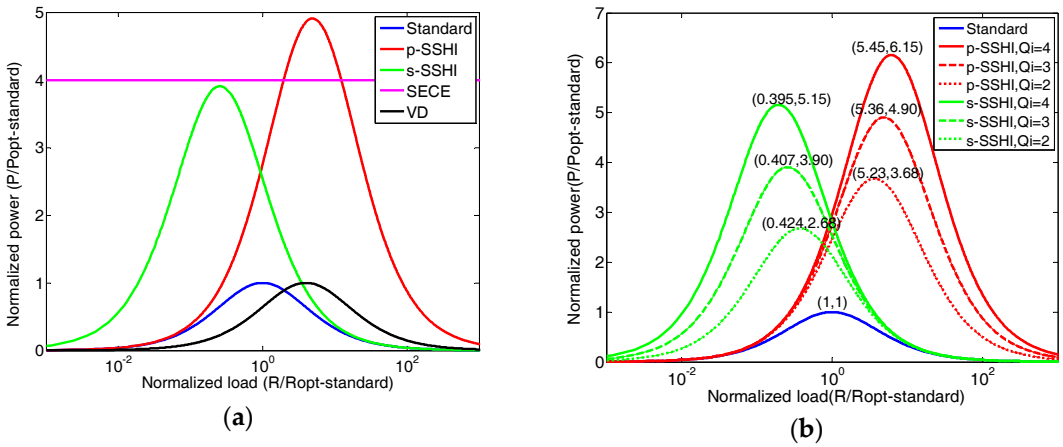

Figure 6. (**a**) Normalized power vs. normalized load in several circuits; (**b**) Q factor effects to SSHI circuits.

2.4. Comparison of interface circuits through simulation and experiments

Figure 7 compares the output characteristics of the standard, p-SSHI and VD circuits after the simulation using PSPICE. Figure 7 (a) shows the output power curves regarding to different loads; the maximum output power of the p-SSHI circuit were 1.95 and 1.98 times respectively larger than the VD circuit and the standard circuit; the maximum output power the VD circuit almost equals to standard circuit, but the optimal load of the VD circuit was almost 10 times greater than the standard circuit. Figure 7 (b) shows the output voltage of three circuits; the output voltage of VD circuit was larger than both p-SSHI and standard circuits.

Preprints (www.preprints.org) | NOT PEER-REVIEWED | Posted: 12 January 2017 doi:10.20944/preprints201701.0062.v1

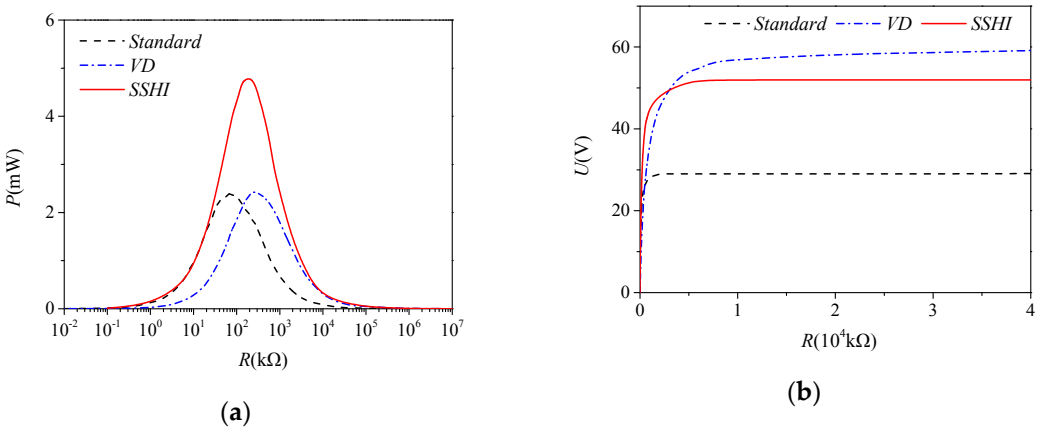

Figure 7. (**a**) Output powers of three circuits in simulation; (**b**) Output voltage of three circuits in simulation.

Above mentioned three circuits were also tested in experiments. Three circuits were mounted in the same PCB board shown in the Figure 8.

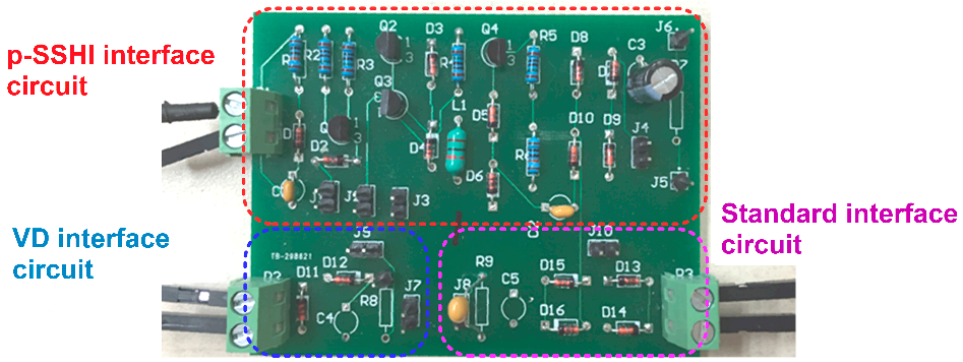

Figure 8. PCB board of three interface circuits

Figure 9 shows the comparison of the experimental results of above three circuits. As can be seen from Figure 9(a), the output power of p-SSHI circuit was maximal and its maximum output power was 1.84 and 1.36 times of the standard and the VD circuits; the optimal load of the p-SSHI circuit was almost 10 times smaller than the VD and standard circuits. From Figure 9(a), we can also see maximum output power of p-SSHI was 3.24mW, which was only 68.2% of the simulation result. These results were different with theoretical and simulation results shown in the Figures 6 and 7. That may be due to following reasons. First, measured output powers of three circuits were lower than the simulation values; it was because a certain power loss existed in the actual circuits. The energy consumption of the p-SSHI circuit was larger than standard and VD circuits, even though the maximum output power of p-SSHI was still larger than VD by 1.35 times. Second, the performance of the p-SSHI circuit was not as good as simulated for both the maximum output power and the optimal load. That may be caused by the leakage resistance of the piezoelectric cantilever itself; parallel inductance L in the circuit also had a certain resistance. The presence of the resistance affected the quality factor of the LC oscillator circuit. The larger the internal resistance, the smaller the quality factor, thus the smaller the maximum output power and output voltage of the circuit. The optimal load would be also smaller because of the internal resistance. For p-SSHI circuit, it is easier to be affected by its internal resistance since its output power directly relates to the quality factor.

Preprints (www.preprints.org) | NOT PEER-REVIEWED | Posted: 12 January 2017 doi:10.20944/preprints201701.0062.v1

In addition, the maximum output power of VD circuit was equal to the standard interface circuit in theory; however, the actual test results showed that maximum output power of the VD circuit was 1.2 times larger than the standard circuit, which was due to simple structure of the VD circuit. Only two diodes were needed to rectify the AC input in VD, which cause less power loss because of the diode voltage drops. Furthermore, the output voltage of the VD was almost 2 times of the standard circuit, which also reduced the power dissipation since output current was smaller for VD circuit.

There are other factors cause the differences between the actual experimental results and the theoretical and simulation results, such as the drift of the natural frequency, dielectric constant and equivalent capacitance of the piezoelectric element after a period of time of the vibration. That will cause the output change of the equivalent current source and other parameters in the circuit, resulting in different outputs.

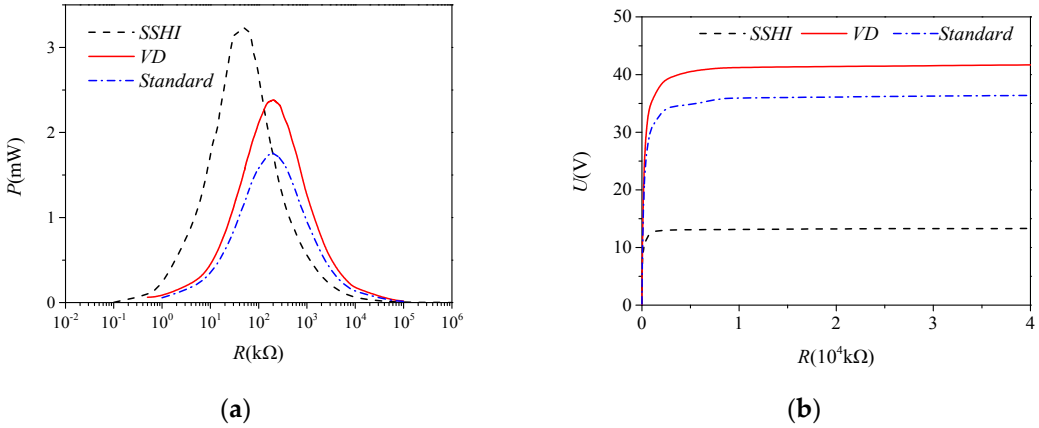

Figure 9. (**a**) Output powers of three circuits in experiments; (**b**) Output voltage of three circuits in experiments.

After the comparison, the VD interface circuit was decided to be applied for the road vibration energy harvesting for its low power dissipation, large optimal load, reasonable output power level, easy control because of the simple structure. We didn't consider the p-SSHI circuit, not only for it is hard to define its quality factor affected by its internal resistance and drift frequency, but also that its control strategy is more complex, and it's hard to realize the goal of 'self-powered'.

3. Results

3.1. Dual mode closed-loop control

The whole energy harvesting circuit was mainly composed of three parts: VD interface circuit, DC-DC converter circuit, and control circuit, which is shown in Figure 10. The VD interface circuit was used for changing the AC voltage after the energy conversion of the PZT to the DC voltage. However, this DC voltage still needs to be further regulated to charge an energy storage battery or super capacitor. DC-DC conversion circuit was used since it could provide higher output efficiency than linear regulator. Here, the buck circuit was used to change the high voltage input of 5-30V to voltage output of 2-3V. The control circuit was to detect the input and output voltages of the VD interface circuit and generate a drive signal for controlling the switch of the Bipolar Junction Transistors (BJTs) in the DC-DC converter circuit. BJTs were selected other than MOSFETs for they consumed less power in this application[21]. Low-power components were used in the control circuit and DC-DC converter circuit to make less power dissipation and achieve self-powered VD energy harvesting circuit.

Preprints (www.preprints.org) | NOT PEER-REVIEWED | Posted: 12 January 2017 doi:10.20944/preprints201701.0062.v1

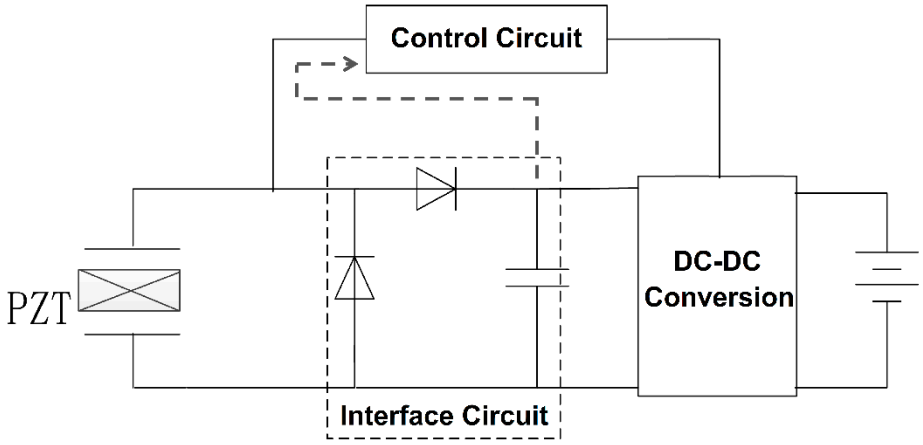

Figure 10. Energy harvesting circuit diagram based on VD interface circuit.

For obtaining high energy conversion efficiency, a control circuit was needed to control the regulation of the DC-DC circuit. There are several control strategies including the PWM, PFM controls for switching on and off the MOSEFT switches normally used in the DC-DC circuit.

PWM is a regulation technique to modify the duty cycle of a fixed-frequency square wave to regulate the output of a power supply; however, PFM technique applies a constant duty cycle and then modulates the square wave's frequency to achieve regulation. There are two kinds of PFM architectures, one is the control strategy of constant-on-time or constant-off-time [33, 34]. The second PFM architecture is a so-called 'hysteretic voltage' control using a simple 'voltage threshold' regulation to switch on and off MOSFETs. It is also referred to as a 'ripple regulator' or 'bang-bang controller' since it continuously shuttles the output voltage back and forth to just above or below the set point. This control strategy is simple, predictable, and could avoid the switch chatter.

PFM strategy offers advantages of better low-power conversion efficiency, lower total solution cost, and simple converter topologies that do not require control-loop-compensation networks. However, it is less popular than PWM control due to notable drawbacks such as the EMI problem produced by the control in a wide frequency range; varied frequency control also causes greater output voltage ripples and a filtering circuit must be considered in the circuit design. The circuit response is also slow when operating at low frequency.

Now, manufacturers offer the 'dual-mode' control, which can automatically shift from the popular pulse width modulation (PWM) regulation method to a pulse frequency modulation (PFM) in different situations[35-42]. This kind control combines the merits of the PWM architecture with those of the PFM, offering a solution with high efficiency across its entire operating range. In high load current, this control switch to the PWM strategy since PWM technique is efficient for moderate to high output power; under low loads, PFM control is employed to increase the efficiency since the switching loss will dominate in that case. TI company applied a DCS control (Direct Control with Seamless Transition) technique to make the control mode transition seamless, greatly improved the conversion efficiency[43]. Other 'dual-mode' control, such as the combination of PSM and PWM have also been applied[44]. At very light loads, some DC-DC converters go into a special form of PFM, referred as 'Power Saving Mode' (PSM) by stopping the oscillator to send the switching pulses. So, it also referred as 'Pulse Skipping Mode'. The PSM control keeps sending constant frequency constant width (CFCW) pulses until the actual voltage exceeds the reference voltage [45].

The hysteretic control is simpler than the voltage or current mode closed-loop control DC-DC switchers, although its simplicity may be a bit deceiving due to component variations and potential sources of "injected" feedback voltage[46]. However, the closed loop control can

Preprints (www.preprints.org) | NOT PEER-REVIEWED | Posted: 12 January 2017 doi:10.20944/preprints201701.0062.v1

still improve its output performance [46]. Closed loop control was applied with either feedback structure by connecting the output with the control circuit or feed-forward structure by connecting the input with the control circuit; most of them used the feedback from the output voltage or current to control the regulation. For example, in the PWM control, the output voltage will be compared with a reference voltage through an error amplifier, and then a triangular wave will be modulated with the output of the amplifier to get the rectangular pulses with a certain duty cycle. There was also the control method by using the input voltage of the DC-DC circuit as a reference voltage to modulate a triangular wave whose amplitude proportional to the output voltage [47].

There were harvester applications based on VD circuit by using the open-loop control method[21, 22]; however, this open loop control strategy is not suitable to the energy harvesting application with the batteries or capacitors for the energy storage. Based on this open-loop controlled circuit, a new closed loop control method was developed in our application.

3.2. Design of the adaptive self-powered harvesting circuit

Figure 11 shows the details of the whole circuit. The control circuit was composed of three low-power comparators of U_1, U_2 and U_3. Low power MAX924 chip with built-in reference voltage of 1.182V was applied, which can be single supplied by a voltage in the range of 2.5~11V. The circuit is called 'self-powered' since these comparators can be supplied by the rechargeable battery in the circuit. The rechargeable battery was used for the energy storage with the output voltage of 2.5V (Riester 10681). We chose the nickel-metal hydride (Ni-MH) type battery for its high energy density (60~80Wh/kg), fast charge and discharge rate. For the charging mode, the mode of constant voltage/current limiting (CV/CL) was applied [48].

D_4 was a schottky diode with voltage drop of only 0.4V. Suppose the battery voltage is V_b. When the voltage across C_r is greater than V_b+0.4V, the circuit starts to charge the rechargeable battery; when the C_r voltage is lower than V_b, D_4 can prevent the energy flow back from the rechargeable battery to DC-DC circuit. Resistor R_9 was a small resistor used to measure the charge current of the rechargeable battery to calculate the power delivered by the circuit.

Preprints (www.preprints.org) | NOT PEER-REVIEWED | Posted: 12 January 2017 doi:10.20944/preprints201701.0062.v1

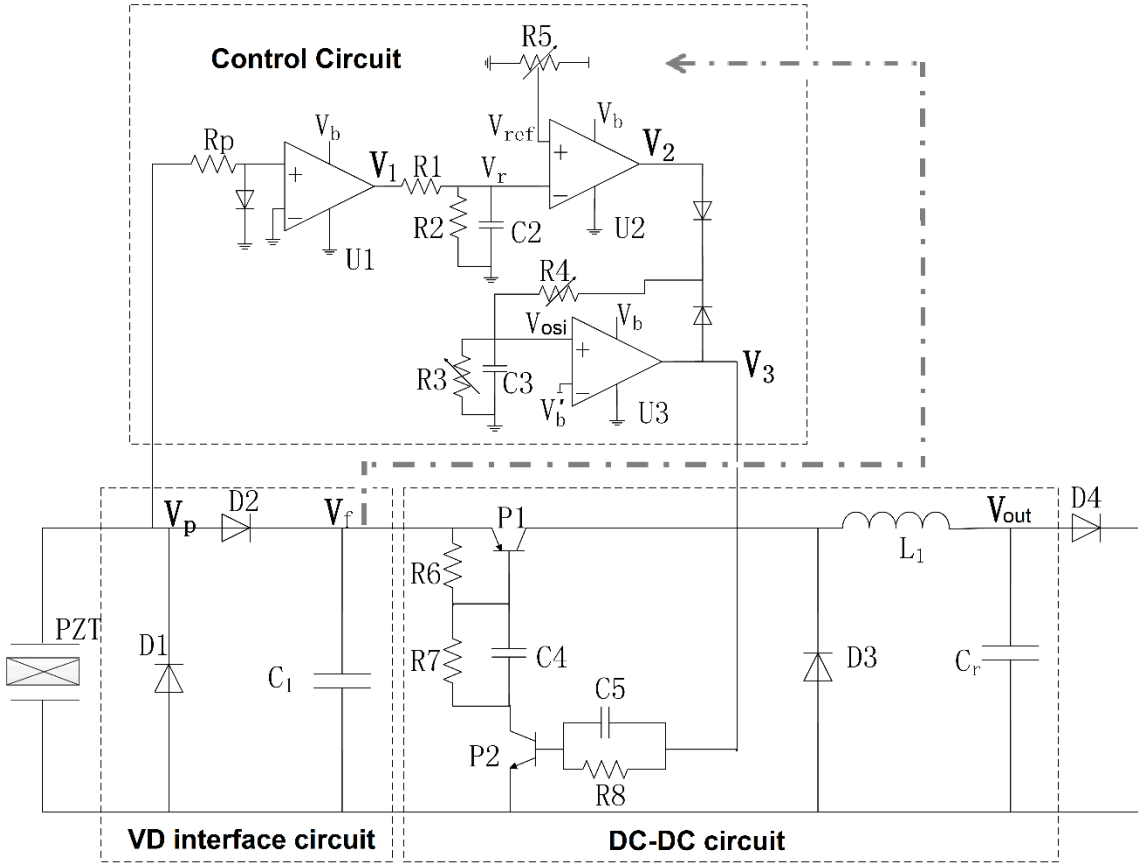

Figure 11. Energy harvesting circuit with VD interface based on closed loop control.

From Figure 12, we can see the VD circuit works mainly in two stages, only one of the diodes D_1, D_2 conducts in a certain time and then another diode will conduct. The period of the third stage when both of them will be cut-off caused by the reverse standoff voltage of the diode is very short. When D_2 turns on, the input voltage V_p equals to the voltage V_f across C_1 plus the voltage drop V_d of D_2. In this stage, V_p is larger than zero. When D_1 turns on, V_p equals to minus V_d, which is smaller than zero. Therefore, when D_2 is turned on, the output voltage V_1 of U_1 is in high level. When D_1 is turned on, V_1 is low. So V_1 is a rectangular wave, its high level stage corresponds to conduction stage of D_2 (the third stage is also in this period), and the low stage corresponds to conduction stage of D_1. R_1, R_2, and C_2 form a low-pass filter. However, it is not a necessary part. By using it, the output voltage of the DC-DC circuit will have fewer ripples. U_2 compares the filtered voltage Vr with a reference voltage V_{ref} to produce a square wave with adjustable duty cycle. If the reference voltage value is below the peak of the V_r, then the output of U_2 is low and that will start the oscillator U_3. When the reference voltage is intersected with V_r, U_3 will only be excited in the period when reference voltage is lower than the V_r. By adjusting the value of R_5, the duty cycle of the output V_2 of U_2 will change with the varied values of the reference voltage V_{ref}; the oscillation period of U_3 will also be changed. The oscillation frequency can be changed by tuning R_4 and R_3.

An N-type BJT P_1, and a P-type BJT P_2 were used as the switch in the DC-DC converter circuit. When the output voltage V_3 of U_3 is high, P_2 turns on and drives P_1 to conduct; when V_3 is low, P_1 will be turned off.

Preprints (www.preprints.org) | NOT PEER-REVIEWED | Posted: 12 January 2017 doi:10.20944/preprints201701.0062.v1

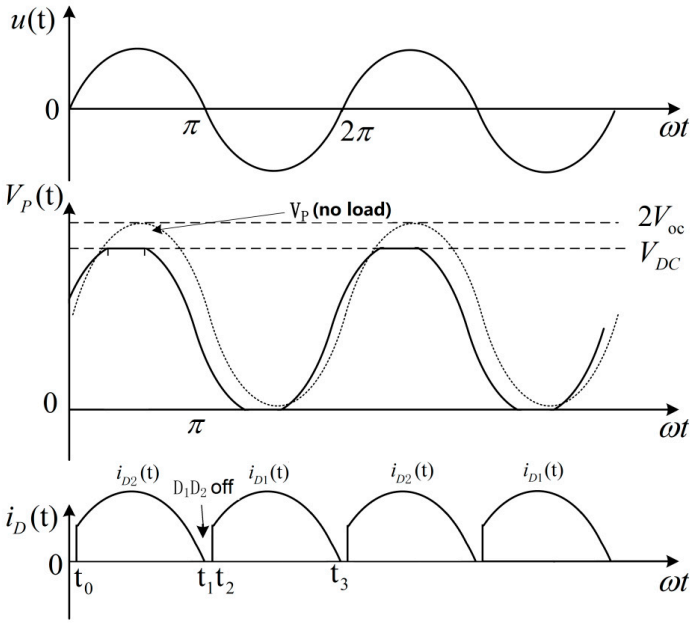

Figure 12. Displacement, input voltage and diode currents of the circuit.

For generating the oscillation, a comparator was used. Its schematic, and its input and output are shown in Figure 13. For the comparator without built-in hysteresis, the feedback needs to be added to the non-inverting input to build an external hysteresis, making the oscillator U_3 work stably. If the values of three resistors R_{10}, R_{11} and R_{12} the same, then the capacitor C_3 will be charged and discharged between $1/3V_{cc}$ and the $2/3V_{cc}$. Here, V_{cc} is the power supply of the chip and equals to V_b since the circuit was self-powered. When the C_3 is charged, V_3 is in high level. However, the value of the charge voltage should minus the voltage drop of the diode. The charge time constant in this period of time is $(R_3//R_4)*C_3$. For the discharge stage of C_3, the time constant is R_3*C_3. After we know the time constants, initial voltage values and final values of C_3, the time duration of each period can be calculated, and the oscillation frequency can be known. For example, When R_4=10kΩ, R_3=50MΩ, then the oscillation frequency is around 260Hz. Voltage waveforms regulated by this frequency are shown in Figure 14. When R_4=200kΩ, R_3=9.8MΩ, oscillation frequency is around 1.4 kHz. Voltage waveforms regulated by this frequency are shown in Figure 15. By changing the values of R_3 and R_4, we can change the oscillation frequency.

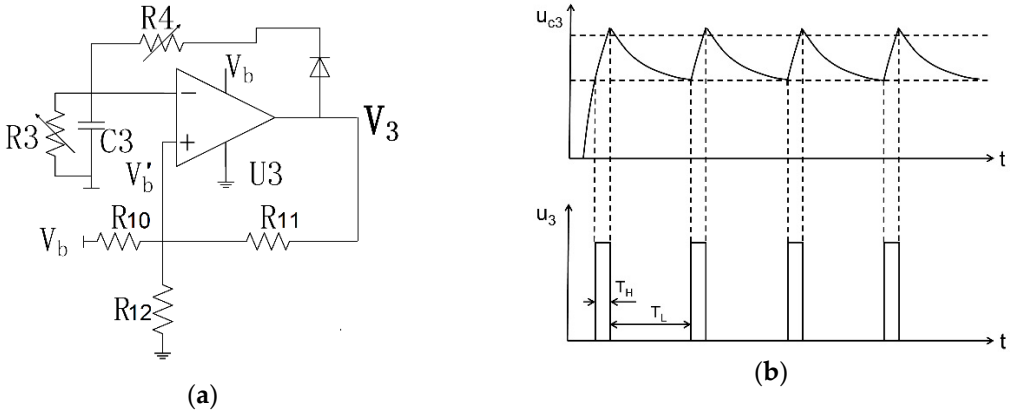

Figure 13. (**a**) Oscillator schematic; (**b**) Input and output voltages of the oscillator.

Preprints (www.preprints.org) | NOT PEER-REVIEWED | Posted: 12 January 2017 doi:10.20944/preprints201701.0062.v1

As aforementioned, the duty cycle of V_3 can be changed by adjusting R_5, thereby the output voltage of DC-DC circuit can be regulated.

Theoretically, when the average voltage V_f on C_1 equals to the open-circuit voltage of the piezoelectric beam, the output power of the circuit reaches the maximum value [21, 45]. In the open-loop control of the circuit based on VD, by adjusting V_{ref}, the duty cycle of V_p will continuously be monitored until it reaches the value of 60% to achieve the maximum output power[21]. However, this control method is not suitable for the circuit with an energy storage element. When the reference voltage is set, the oscillator will work at least for a certain time in one cycle if we need to charge the battery, and there is no method to stop the charge of C_r and the battery. The discharge of the battery through Cr is not allowed. Now, the battery will face the danger of overcharge.

Waveforms of V_f are shown in Figures 14(a) and 15(a). After passing through a voltage divider, which is an adjustable shunt resistor R_5, V_f will become the reference voltage V_{ref}. V_{ref} will be compared with the square wave V_r shown in Figures 14(b) and 15(b). In our closed-loop application, we can see V_f is a triangular waveform other than a relatively constant DC voltage in the open-loop control. The triangular shape of V_f corresponds to the charge and discharge of C_1, stages of obtaining the energy from the piezoelectric element and then passing it to the DC-DC circuit. When the input voltage V_p changes, both V_r and V_f will follow its change, thus the cycle duty of V_2 will be locked and DC-DC output V_{out} keeps constant. From this point view, the circuit is 'adaptive'.

In addition, this circuit can work in two different modes. The first control mode is similar with the PWM control. The second control mode is the combination of the PWM and the PSM control.

The first control mode is actually in a critical condition, that is, the reference voltage V_{ref} is just slightly lower than V_r, and thus the duty cycle of V_2 will be large. V_{ref} , V_r and V_2 are shown in Figure 14(b). Even though the oscillator will be enabled in the low level stage of V_2, the time is short enough to allow only one pulse to switch on P_2 in each cycle. From the waveform of V_{osi} in Figure 14 (b), we can see there is only one oscillation in its active stage, resulting in V_3 has only one switch pulse in each cycle shown in Figure 14(a).

In the second control mode shown in Figure 15, the oscillator will send many pulses during the active stage, which is similar to the PSM control. However, the overall control is still based on the PWM control.

The regulated output voltages V_{out} varied depending on the reference voltage and the oscillation frequency. To increase the output voltage, we can either decrease the reference voltage by adjusting R_5, or increase the oscillation frequency, which will make U_3 send out more pulses to switch on P_2. Reference voltages in Figures 13 and 14 were the same; however, the oscillation frequencies were different. We can see the amplitude of the output V_{out} is higher for oscillation with high frequency than the low frequency one.

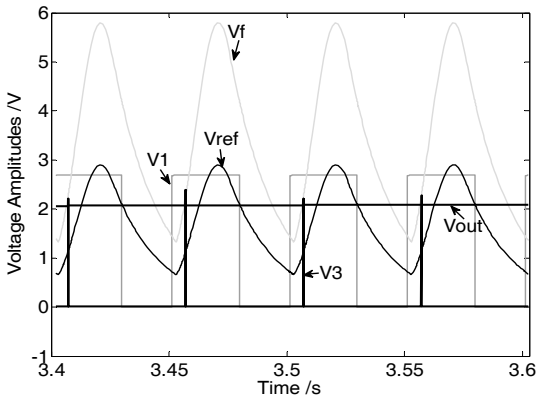

(**a**)

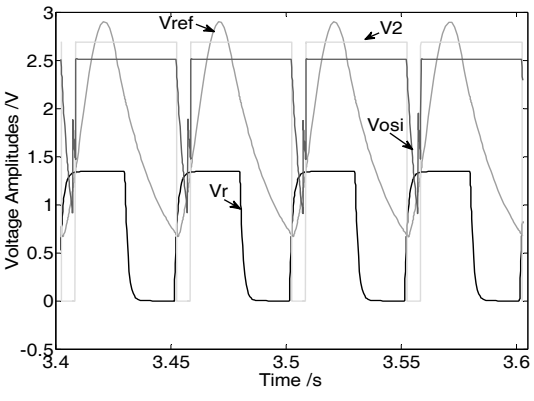

(**b**)

Preprints (www.preprints.org) | NOT PEER-REVIEWED | Posted: 12 January 2017 doi:10.20944/preprints201701.0062.v1

Figure 14. Voltage signals when oscillation frequency was 260Hz: (**a**) V_1, V_f, V_{ref}, V_3 and V_{out}; (**b**) V_r, V_{ref}, V_2 and V_{osi}. .

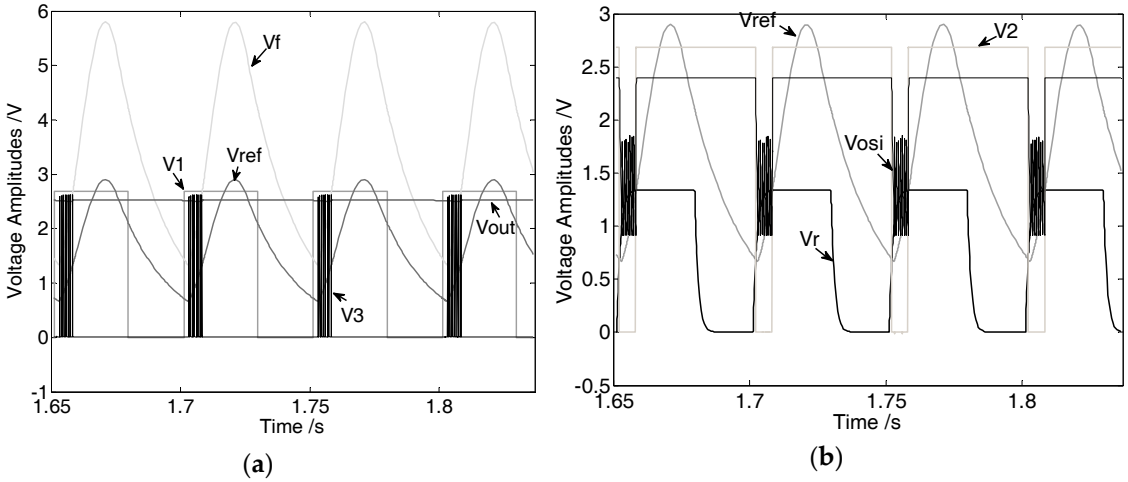

Figure 15. Voltage signals when oscillation frequency was 1.4kHz: (**a**) V_1, V_f, V_{ref}, V_3 and V_{out}; (**b**) V_r, V_{ref}, V_2 and V_{osi}.

Figure 16 shows the V_{out} signals when changing the reference voltage V_{ref} and oscillation frequency. Figure 16 (a) shows the V_{out} increased with the decrease of V_{ref} when oscillation frequency was 260Hz; Figure 16 (b) also shows the increase of V_{out} with the decrease of V_{ref} when oscillation frequency was 1.4kHz. However, the transient state was longer before V_{out} reaches to stable when the oscillation frequency was low. However, there were more ripples in the V_{out} when the oscillation frequency was high. There is the tradeoff between the transient responses and the stable responses.

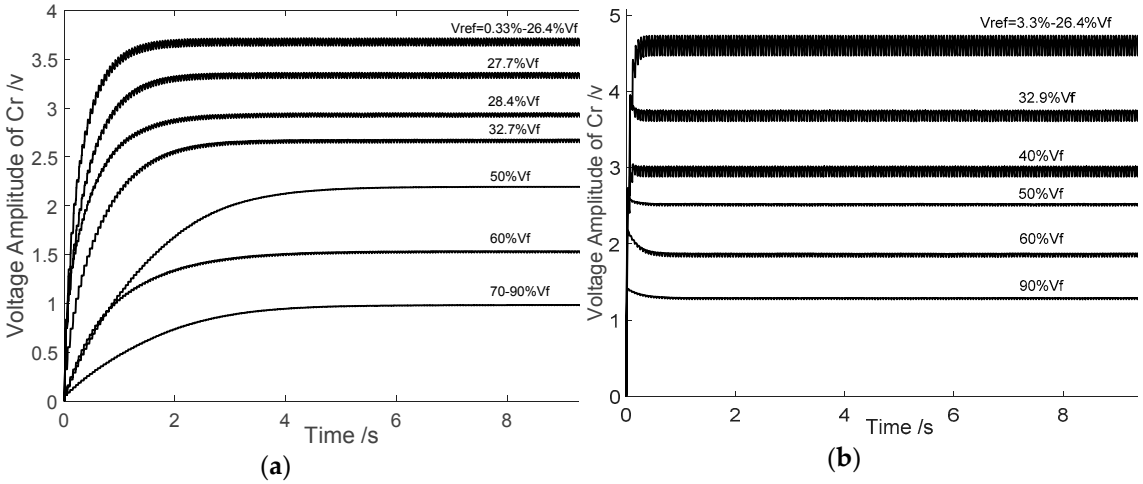

Figure 16. Voltage signals of Vout: (**a**) When oscillation frequency was 260Hz; (**b**) When oscillation frequency was 1.4kHz.

Furthermore, the value of the voltage divider R_5 should be chosen carefully since it can directly affects the value of V_{ref}. Figure 17 shows the effects of R_5 to the output V_{out}. When R_5 has a larger value of 20kΩ , the ripples of V_{out} will be smaller than the ones when R_5 equals 10kΩ.

Preprints (www.preprints.org) | NOT PEER-REVIEWED | Posted: 12 January 2017 doi:10.20944/preprints201701.0062.v1

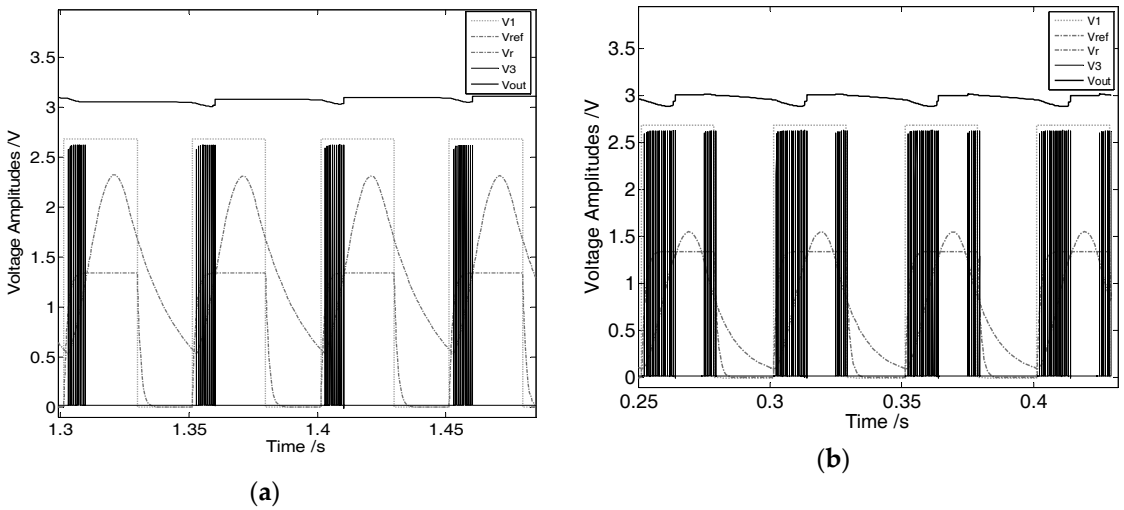

Figure 17. Voltage signals of V_1, V_{ref}, V_r, V_3 and V_{out}: (**a**) When R_5 was 20kΩ; (**b**) When R_5 was 10kΩ.

However, the oscillation frequency shouldn't be too high even though it has better transient response in this case. Not only because it will increase the output ripples, but also it will affects the output efficiency of the whole circuit. In the high frequency regime, switch loss will dominate the power dissipation. Switch frequency is better below 100 kHz for the low power vibration energy harvesting application [49, 50].

In this new approached control method, multi pulses will be excited when V_{ref} is lower than V_r. It is similar to the 'Multi-shot technology' [51]. In the multi-shot technology, multi switching shots with small duty-cycles were used other than a single switching shot. Using this technique, not only the size of the DC-DC circuit will be smaller[49], but also the power loss will be reduced to $\sqrt{N}$ [51]. The conduction losses are approximately divided by $\sqrt{N}$ since the maximum current values are divided by $\sqrt{N}$ compared to the single-shot method [51].

The circuit loss included the control circuit loss, the VD circuit loss and the DC-DC circuit loss. The control loss was composed of low-power comparators and can be estimated according to the chip manual, which was around 50mW.The efficiency of the circuit can be calculated using the output power divided by the input power. The input powers and output powers when changing the average value of V_f are shown in the Figure 18. Thus, the circuit efficiency was around 20%. The power dissipation was mainly from the voltage divider R_5 for the voltage sensing. By increasing R_5, the power loss will be decreased. In addition, if the output voltage is increased, the power loss will also be decreased.

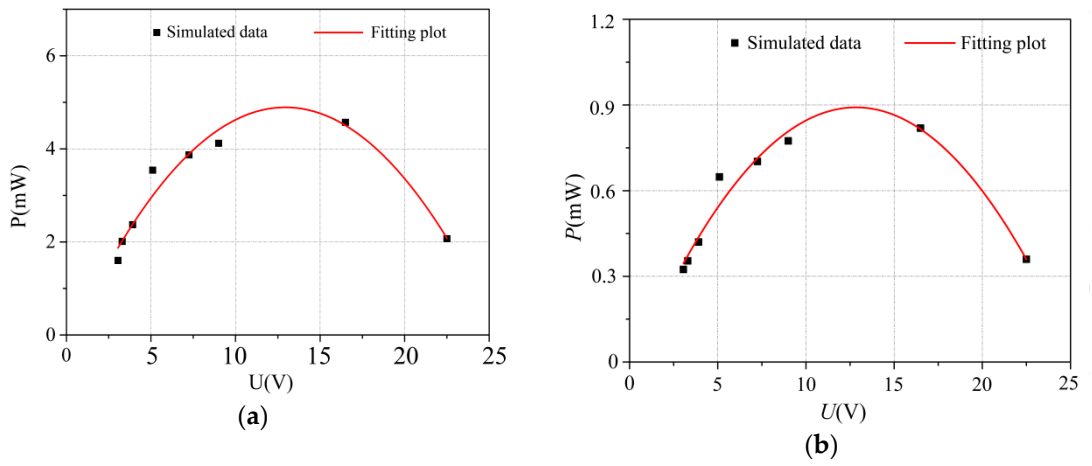

Preprints (www.preprints.org) | NOT PEER-REVIEWED | Posted: 12 January 2017 doi:10.20944/preprints201701.0062.v1

Figure 18. (**a**) Circuit input power when changing the average value of V_f; (**b**) Circuit output power when changing the average value of V_f.

3.4. Experimetnal results of the designed energy harvesting system

Figure 19(a) is the experimental setup of the piezoelectric energy harvesting system. Figure 19(b) shows the PCB board of the harvesting circuit with the new proposed control method. The system consists of two parts; one was the mechanical vibration excitation and control system including the shake table, shake table controller and piezoelectric cantilever beam. The shake table WS-Z30-50 was used for the vibrating the piezoelectric cantilever beam under the control of the controller according to the set displacement amplitude of 0.02mm and frequency of 20Hz with the vibrating time period of 100s. As shown in Figure 1, the piezoelectric material was adhered to the surface of the thin copper plate with a conductive paste. The proof mass at the end of the cantilever has the mass of 13.6g. The natural frequency and capacitance of the piezoelectric element were measured before the experiment. The first-order natural frequency of the beam was about 21Hz and the capacitance was around 150nF. As the piezoelectric material is fragile, one end of the piezoelectric cantilever beam was tightly fixed in the shaking table. Also, a small frequency offset was set to the first order natural frequency in the beginning to prevent the damage of the beam because of large vibration. The other part of the system was the energy harvesting and testing part, including the integrated energy harvesting circuit, the data acquisition card(HS4), the oscilloscope(TDS2024B) and the variable resistance. The variable resistor box was used to change the load. Piezoelectric cantilever output voltage was 30V by slowly adjusting the vibration gain of the controller.

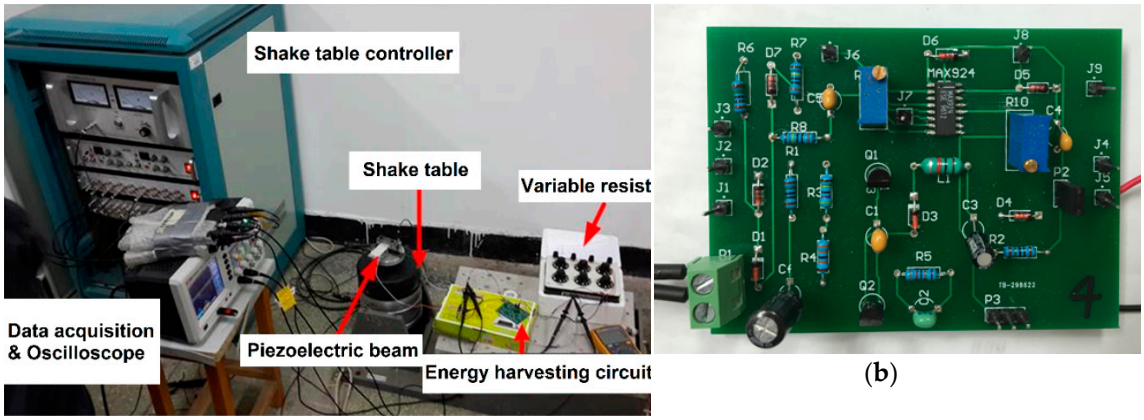

(**a**) (**b**)

Figure 19. (**a**) Experimental setup; (**b**) PCB board of the circuit.

Figure 20 shows the output waveform of the DC-DC output. The maximum output power of the circuit was 0.78mW. The measured input power was about 4.89mW, thus the efficiency of the circuit was about 16%.

 doi:10.20944/preprints201701.0062.v1

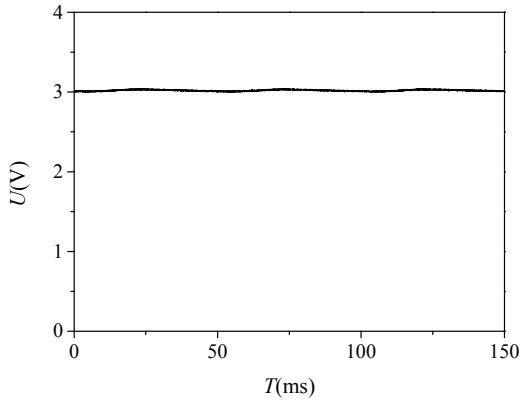

Figure 20. Output voltage of the harvesting circuit based on VD.

4. Discussion

A piezoelectric cantilever beam capture device was designed firstly and applied to scavenge the vibration energy of the bridge road. Then several interface circuits have been compared through numerical calculation, simulation and experiment test. Differences existed between the theoretical, simulation and experimental values because of the leakage resistance of the piezoelectric beam, the frequency drift caused by the parameter variation, and the power loss. The performances of the SECE and SSHI circuits in real case were not as good as the ideal circuits. Furthermore, their control strategies were complex and it is hard to realize the goal of 'self-powered'. The VD circuit was simple and easy to be controlled.

In this paper, a new closed loop control method was proposed based on the VD interface circuit. This circuit sensed the DC-DC input voltage as the feed-forward signal to adjust the switching duration. If the input voltage was too high, then the oscillator would not be activated. By using multi-shots technique, the output loss can be reduced. Parameters of the oscillator could be adjusted to change the pulse 'on' and 'off' duration and the oscillation frequency. Pulse with short duty cycle was preferred for reducing the size of DC-DC circuit and improve the output efficiency. Overall, the closed-loop was similar to the PSM control based on PWM. This dual-mode control could improve the output efficiency of the circuit. In addition, this closed-loop control was an adaptive, self-powered, autonomous method.

However, we should note here, the output efficiency was 40% less than the efficiency of the open-loop circuit. Harvested power was only 0.78mW with the efficiency of 16% by using this control strategy. The power loss was caused mainly by the voltage sensing resistor. The value of the shunt resistor should not be too small to pass through larger current, causing larger power loss. Furthermore, by increasing the output voltage, the efficiency can be greatly improved.

In summary, the proposed circuit has an acceptable efficiency; in addition, it is adaptive, self-powered, and stand-alone. The power supply demand of wireless sensors in the bridge can be satisfied by applying this circuit.

Acknowledgments: The project is supported by National Natural Science Foundation of China (Grant no. 61307123) .

References

1. Kymissis, J., Kendall, C., Paradiso, J., and Gershenfeld, N., Parasitic Power Harvesting in Shoes, in Proceedings of the 2nd IEEE International Symposium on Wearable Computers 1998, IEEE Computer Society. p. 132.
2. Shenck, N.S. and Paradiso, J.A., Energy scavenging with shoe-mounted piezoelectrics. *IEEE Micro* **2001**, 21(3): p. 30-42.
3. Roundy, S. and Wright, P.K., A piezoelectric vibration based generator for wireless electronics. *Smart Materials and Structures* **2004**, 13(5): p. 1131.
4. Spencer, B.F., Ruiz-Sandoval, M.E., and Kurata, N., Smart sensing technology: opportunities and challenges. *Structural Control and Health Monitoring* **2004**, 11(4): p. 349-368.
5. Percy, S., Knight, C., Cooray, F., and Smart, K., Supplying the Power Requirements to a Sensor Network Using Radio Frequency Power Transfer. *Sensors (Basel, Switzerland)* **2012**, 12(7): p. 8571-8585.
6. Jain, A. and Bhullar, S., Emerging Dimensions in the Energy Harvesting, in *IOSR JOURNAL OF ELECTRICAL AND ELECTRONICS ENGINEERING* **2012**. p. 70-80.
7. Kim, S.-W., Cho, I., Lee, J.-H., Park, J., Yi, D.-H., and Cho, D.D., A New Method for Accurately Estimating the Weight of Moving Vehicles Using Piezoelectric Sensors and Adaptive-footprint Tire Model. *Vehicle System Dynamics* **2003**, 39(2): p. 135-148.
8. Galchev, T.V., McCullagh, J., Peterson, R.L., and Najafi, K., Harvesting traffic-induced vibrations for structural health monitoring of bridges. *Journal of Micromechanics and Microengineering* **2011**, 21(10): p. 104005.
9. Yu, J., Jize, Y., Tao, F., Sijun, D., Paul, F., Kenichi, S., Campbell, M., and Ashwin, A.S., A vibration powered wireless mote on the Forth Road Bridge. Journal of Physics: Conference Series, 2015, 660(1): p. 012094.
10. Yuan, F.-G., Structural Health Monitoring (SHM) in Aerospace Structures. Elsevier. 2016.
11. Lallart, M. and Inman, D., Mechanical effect of combined piezoelectric and electromagnetic energy harvesting. In: Structural dynamics and renewable energy. Springer. New York: 2011; Vol. 1. 261–272.
12. Hooker, M.W., Properties of PZT-Based Piezoelectric Ceramics Between -150 and 250 °C, 1998.
13. Priya, S. and Inman, D.J., Energy Harvesting Technologies. Springer Publishing Company, Incorporated: 2008524.
14. Ottman, G.K., Hofmann, H.F., Bhatt, A.C., and Lesieutre, G.A., Adaptive piezoelectric energy harvesting circuit for wireless remote power supply. *IEEE Transactions on Power Electronics* **2002**, 17(5): p. 669-676.
15. Williams, C.B. and Yates, R.B., Analysis of a micro-electric generator for microsystems. *Sensors and Actuators A: Physical* **1996**, 52(1–3): p. 8-11.
16. Lefeuvre, E., Sebald, G., Guyomar, D., Lallart, M., and Richard, C., Materials, structures and power interfaces for efficient piezoelectric energy harvesting. *Journal of Electroceramics* **2009**, 22(1): p. 171-179.
17. Taylor, G.W., Burns, J.R., Kammann, S.A., Powers, W.B., and Welsh, T.R., The Energy Harvesting Eel: a small subsurface ocean/river power generator. *IEEE Journal of Oceanic Engineering* **2001**, 26(4): p. 539-547.
18. Lefeuvre, E., Badel, A., Benayad, A., Lebrun, L., Richard, C., and Guyomar, D., A comparison between several approaches of piezoelectric energy harvesting. *J. Phys. IV France* **2005**, 128: p. 177-186.
19. Mickaël, L. and Daniel, G., An optimized self-powered switching circuit for non-linear energy harvesting with low voltage output. *Smart Materials and Structures* **2008**, 17(3): p. 035030.
20. Chen, Y.-Y., Vasic, D., Costa, F., Lee, C.-K., and Wu, W.-J., Self-powered semi-passive piezoelectric structural damping based on zero-velocity crossing detection. *Smart Materials and Structures*, **2013**, 22(2): p. 025029.
21. Tabesh, A. and Frechette, L.G., A Low-Power Stand-Alone Adaptive Circuit for Harvesting Energy From a Piezoelectric Micropower Generator. *IEEE Transactions on Industrial Electronics* **2010**, 57(3): p. 840-849.
22. Tabesh, A. and Fréchette, L.G. Ultra Low Power Stand-alone Circuitry for Harvesting Energy from a Micro-power Piezoelectric Generator. in Proceedings of PowerMEMS+microMEMS. 2009.

23. Zhao, H., Yu, J., and Ling, J., Finite element analysis of Cymbal piezoelectric transducers for harvesting energy from asphalt pavement. *Journal of the Ceramic Society of Japan* **2010**, 118(1382): p. 909-915.
24. Zhao, H., Tao, Y., Niu, Y., and Ling, J., Harvesting energy from asphalt pavement by piezoelectric generator. *Journal of Wuhan University of Technology-Mater. Sci. Ed.* **2014**, 29(5): p. 933-937.
25. Michaël, P. and Dominique, S., Piezoelectric energy harvesting from traffic-induced bridge vibrations. *Smart Materials and Structures* **2013**, 22(9): p. 095019.
26. Wang, J., Shi, Z., Xiang, H., and Song, G., Modeling on energy harvesting from a railway system using piezoelectric transducers. *Smart Materials and Structures* **2015**, 24(10): p. 105017.
27. Steven, R.A. and Henry, A.S., A review of power harvesting using piezoelectric materials (2003–2006). *Smart Materials and Structures* **2007**, 16(3): p. R1.
28. Bhanusri, E.V.M. Design and Simulation of Unimorph Piezoelectric Energy Harvesting System. in Proceedings of the 2013 COMSOL Conference Bangalore.
29. Guyomar, D. and Lallart, M., Recent Progress in Piezoelectric Conversion and Energy Harvesting Using Nonlinear Electronic Interfaces and Issues in Small Scale Implementation. *Micromachines* **2011**, 2(2): p. 274.
30. Dicken, J., Mitcheson, P.D., Stoianov, I., and Yeatman, E.M., Power-Extraction Circuits for Piezoelectric Energy Harvesters in Miniature and Low-Power Applications. *IEEE Transactions on Power Electronics* **2012**, 27(11): p. 4514-4529.
31. Lefeuvre, E., Badel, A., Richard, C., and Guyomar, D., Energy harvesting using piezoelectric materials: Case of random vibrations. *Journal of Electroceramics* **2007**, 19(4): p. 349-355.
32. Guyomar, D., Badel, A., Lefeuvre, E., and Richard, C., Toward energy harvesting using active materials and conversion improvement by nonlinear processing. *IEEE Transactions on Ultrasonics, Ferroelectrics, and Frequency Control* **2005**, 52(4): p. 584-595.
33. Hsu, K.Y., Reduction of Parasitic Component Effect in Constant On-Time Control for Buck Converter with Multi-layer Ceramic Capacitors. National Chiao Tung University, Taiwan: 2012.
34. Safari, N., Design of a DC/DC buck converter for ultra-low power applications in 65nm CMOS Process, in Department of Electrical Engineering, Electronic Devices 2012, Linköping University,.
35. Kapat, S., Mandi, B.C., and Patra, A., Voltage-Mode Digital Pulse Skipping Control of a DC-DC Converter With Stable Periodic Behavior and Improved Light-Load Efficiency. *IEEE Transactions on Power Electronics* **2016**, 31(4): p. 3372-3379.
36. Shrivastava, A. and Calhoun, B., A DC-DC Converter Efficiency Model for System Level Analysis in Ultra Low Power Applications. *Journal of Low Power Electronics and Applications* **2013**, 3(3): p. 215.
37. Zhen, S., Zhang, B., Luo, P., Hou, S., Ye, J., and Ma, X., A digitally controlled PWM/PSM dual-mode DC/DC converter. *Journal of Semiconductors* **2011**, 32(11): p. 115007.
38. Chen, Y. and Kang, Y., The Variable-Bandwidth Hysteresis-Modulation Sliding-Mode Control for the PWM/PFM Converters. *IEEE Transactions on Power Electronics* **2011**, 26(10): p. 2727-2734.
39. Kim, J., Chu, H., and Kim, C. Current-mode DC-DC buck converter with reliable hysteretic-mode control and dual modulator for fast dynamic voltage scaling. in 2009 52nd IEEE International Midwest Symposium on Circuits and Systems. 2009.
40. Zhang, X. and Maksimovic, D. Digital PWM/PFM controller with input voltage feed-forward for synchronous buck converters. in 2008 Twenty-Third Annual IEEE Applied Power Electronics Conference and Exposition. 2008.
41. Wang, J., Gong, W., and He, L. Design and implementation of high-efficiency and low-power DC-DC converter with PWM/PFM modes. in 2007 7th International Conference on ASIC. 2007.
42. Hamamura, S., Ninomiya, T., Yamamoto, M., and Katsuno, M., Combined PWM and PFM control for universal line voltage of a piezoelectric transformer off-line converter. *IEEE Transactions on Power Electronics* **2003**, 18(1): p. 270-277.
43. Glaser, C. High-efficiency, low-ripple DCS-Control™ offers seamless PWM/power-save transitions. *Analog Applications Journal* **2013**.
44. Cheng, J., Ma, Z., and Zhang, H., A voltage mode buck DC–DC converter with automatic PWM/PSM mode switching by detecting the transient inductor current. *Analog Integrated Circuits and Signal Processing* **2014**, 80(2): p. 243-253.

45. Ramamurthy Srinivasan; Vanaja Ranjan, P., "Pulse Skipping Modulated Buck Converter - Modeling and Simulation. *Circuits and Systems* **2010**, 1(2): p. 59-64.
46. Daugherty, K. Feedback Circuit Improves Hysteretic Control. National Semiconductor: *Power Electronics* **2008**.
47. Cao, X., Chiang, W.J., King, Y.C., and Lee, Y.K., Electromagnetic Energy Harvesting Circuit With Feedforward and Feedback DC–DC PWM Boost Converter for Vibration Power Generator System. *IEEE Transactions on Power Electronics* **2007**, 22(2): p. 679-685.
48. Rangan, C.S., Sarma, G.R., and Mani, V.S.V., Instrumentation Devices and Systems. Tata McGraw-Hill Education: 1997.
49. Tod, P., Short Duty Cycles Lead to Smaller DC-DC Converters, 2009, Allegro Microsystems.
50. Ottman, G.K., Hofmann, H.F., and Lesieutre, G.A., Optimized piezoelectric energy harvesting circuit using step-down converter in discontinuous conduction mode. *IEEE Transactions on Power Electronics* **2003**, 18(2): p. 696-703.
51. Gasnier, P., Willemin, J., Boisseau, S., Despesse, G., Condemine, C., Gouvernet, G., and Chaillout, J.J., An Autonomous Piezoelectric Energy Harvesting IC Based on a Synchronous Multi-Shot Technique. *IEEE Journal of Solid-State Circuits* **2014**, 49(7): p. 1561-1570.